

## Gram-negative and Gram-Positive Bacterial Infections Give Rise to a Different Metabolic Response in a Mouse Model

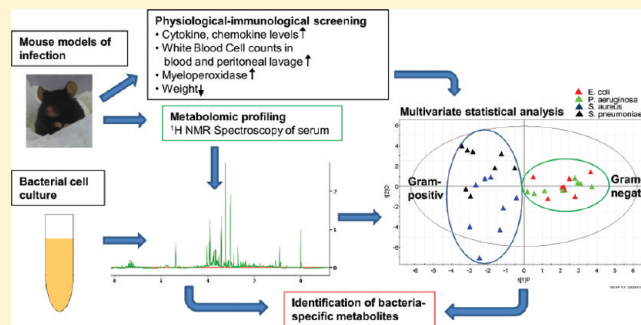
Verena Hoerr,<sup>†,§</sup> Lori Zbytnuik,<sup>‡</sup> Caroline Leger,<sup>‡</sup> Patrick P.C. Tam,<sup>‡</sup> Paul Kubes,<sup>‡</sup> and Hans J. Vogel<sup>\*,†</sup>

<sup>†</sup>Biochemistry Research Group, Department of Biological Sciences, <sup>‡</sup>Department of Physiology and Biophysics, Snyder Institute, University of Calgary, Calgary, Alberta T2N 1N4, Canada

Supporting Information

**ABSTRACT:** Metabolomics has become an important tool to study host-pathogen interactions and to discover potential novel therapeutic targets. In an attempt to develop a better understanding of the process of pathogenesis and the associated host response we have used a quantitative <sup>1</sup>H NMR approach to study the metabolic response to different bacterial infections. Here we describe that metabolic changes found in serum of mice that were infected with *Staphylococcus aureus*, *Streptococcus pneumoniae*, *Escherichia coli* and *Pseudomonas aeruginosa* can distinguish between infections caused by Gram-positive and Gram-negative bacterial strains. By combining the results of the mouse study with those of bacterial footprinting culture experiments, bacterially secreted metabolites could be identified as potential bacterium-specific biomarkers for *P. aeruginosa* infections but not for the other strains. Multivariate statistical analysis revealed correlations between metabolic, cytokine and physiological responses. In TLR4 and TLR2 knockout mice, host-response pathway correlated metabolites could be identified and allowed us for the first time to distinguish between bacterial- and host-induced metabolic changes. Since Gram-positive and Gram-negative bacteria activate different receptor pathways in the host, our results suggest that it may become possible in the future to use a metabolomics approach to improve on current clinical microbiology diagnostic methods.

**KEYWORDS:** metabolomics, <sup>1</sup>H NMR spectroscopy, Gram-negative and Gram-positive bacterial infections, bacteria-secreted metabolites, knockout mice, host response, metabolic responses, physiological responses, cytokine responses, multivariate data analysis



### INTRODUCTION

The emergence of multiple antibiotic-resistant Gram-positive and Gram-negative bacteria in hospital and community settings requires novel approaches for rapid diagnosis and treatment.<sup>1–3</sup> The clinical diagnosis of bacterial infections is currently still mostly based on recovering and culturing of microorganisms from patients' blood or other bodily fluids. Molecular tests to detect infectious agents are increasingly being used in many clinical laboratories; however, they have not yet become part of routine practice. The nonmolecular diagnostic tests lack diagnostic accuracy, are time-consuming, labor-intensive and can give erroneous information, particularly in immunodeficient patients.<sup>4</sup> Most importantly, the tests are not sensitive, and as such at least 50% of bacterial infections go undetected by state of the art clinical methods. These problems have led to an emerging interest in identifying disease specific biomarkers or other physiological indicators that can predict the severity and the nature of bacterial infections. Moreover, collectively, such biological indicators can potentially guide the selection of the optimal antibiotic treatment.<sup>5</sup> For example, recently, procalcitonin, a peptide hormone and cytokine that is mainly produced in response to bacterial infections, was found to be a

convenient diagnostic marker to distinguish between bacterial and viral infections.<sup>4,6</sup> However, a single biomarker has major limitations and is often equivocal. Moreover, to date, the differentiation between infections caused by different bacterial strains is still challenging yet would certainly aid physician treatment decisions.

In recent years, the focus for finding novel diagnostic tools has moved from single disease-specific markers to bioprofiles or biosignatures comprising a well-defined set of reliable molecular indicators<sup>7,8</sup> using platforms such as proteomics,<sup>9</sup> transcriptomics,<sup>10</sup> genomics,<sup>8</sup> and metabolomics.<sup>11</sup> Metabolomics allows researchers to characterize and quantify a plethora of low molecular mass metabolites from biofluids such as urine, serum, and cerebrospinal fluid. Like the other “omics” technologies, metabolomics also relies on systematic data analysis using multivariate pattern recognition techniques.<sup>12–14</sup> NMR metabolomics has been shown to produce highly quantitative and reproducible results.<sup>15</sup> In previous studies aimed at developing new methods for early diagnosis of bacterial infections, the

Received: December 31, 2011

Published: April 9, 2012



NMR-metabolomics approach has already been applied to growing bacterial cultures<sup>16</sup> as well as for the differentiation between bacterial and viral meningitis.<sup>17</sup> Furthermore, different bacterial lower respiratory tract infections have been investigated in mouse models and human patients as well.<sup>18,19</sup>

Metabolomics offers a unique approach to characterize all the metabolic changes that occur in an organism in response to biological and toxicological stimuli.<sup>15,20,21</sup> In the case of infectious diseases, the metabolic profiles of bodily fluids are expected to reflect both the molecules generated by the innate defense response as well as metabolites that are secreted by the pathogens. In addition, host cellular events, such as altered energy metabolism, which are a direct result of the disease, will occur in parallel.

The pathogenicity of bacteria is usually caused by bacterial molecular elements such as toxins, exoenzymes, adhesins, as well as immune-modulating proteins that are released. Many of these PAMPs are recognized by the Toll-like receptor transmembrane protein family which plays a key role in mediating the systemic responses to invading pathogens.<sup>22</sup> In *in vitro* studies specific ligands have been identified for different TLRs such as Gram-negative bacterial lipopolysaccharide for TLR4 and lipoteichoic acid from the Gram-positive cell wall for the TLR2/TLR6 heterodimer.<sup>23,24</sup> While the TLR4-dependent recognition of LPS is very well-established as the central line of host defense against invading Gram-negative pathogens, there is now growing evidence that LTA may in fact activate additional anti-inflammatory properties and pathways.<sup>25,26</sup> Consequently, rather than using LTA, synthetic peptides such as the TLR1/TLR2 agonist Pam<sub>3</sub>Cys and the TLR2/TLR6 agonist MALP2 are used instead to activate these TLRs.

Since Gram-negative and Gram-positive bacteria act on different receptors, we can hypothesize that the host metabolic response will be distinct in each case. The aim of our study is to evaluate this notion. Therefore, in this work we have analyzed serum from mouse models of bacterial infections (*Staphylococcus aureus*, *Streptococcus pneumoniae*, *Escherichia coli*, and *Pseudomonas aeruginosa*) and examined low-molecular-weight pathogen-specific biomarkers through NMR metabolomics. An extensive array of physiological and immunological data was measured to confirm that a systemic infection was established in all cases. To differentiate the metabolites according to their origin, we compared the results of the *in vivo* studies with those obtained in bacterial culture experiments. By comparing serum metabolite changes resulting from LPS or MALP2 treatment of the mice and from studies of TLR4 and TLR2 knockout mice we could identify those metabolites generated by the host response. Finally, we incorporated all the metabolic, physiological, and immunological data into one descriptive model of disease, which showed good correlations between the various parameters.

## MATERIALS AND METHODS

### Bacteria and Growth Conditions

**Bacterial Strains.** Experiments were performed with two Gram-positive bacterial strains (*Streptococcus pneumoniae* (SPN 15814 strain) and *Staphylococcus aureus* (Xen29)) and with two Gram-negative bacteria (*Pseudomonas aeruginosa* (PA01) and *Escherichia coli* (Xen14)). Both the *E. coli* and the *S. aureus* strain (Caliper Life Sciences, Hopkinton, MA) possess a stable copy of the *Phosphorhabdus luminescens lux operon ABCDE* on

the bacterial chromosome which allowed us to monitor the progression of the infection by bioluminescence.

**Cultivation.** Prior to analysis, frozen stock suspensions of bacteria were cultured overnight in 5 mL of Luria-Bertani medium (*S. aureus*, *P. aeruginosa*, *E. coli*) or brain-heart infusion broth (*S. pneumoniae*) at 37 °C with shaking at 200 rpm. To guarantee strain selectivity, media contained kanamycin in an appropriate concentration (200 µg/mL for *S. aureus* and 30 µg/mL for *E. coli*). For the bacterial foot- and fingerprint analysis, 1 mL of the overnight culture was reinoculated into 50 mL of the corresponding culture broth, and bacteria were cultured in 500 mL flasks under the same conditions up to an OD600 (optical density at 600 nm) of 0.6. For each bacterial strain, cultures were prepared in duplicate. For the *in vivo* experiments in mice, 1 mL of the overnight culture was reinoculated into 5 mL of medium and incubated for 3–5 h at 37 °C with shaking at 250 rpm.

**Cell Concentration.** The cell concentration was determined by measuring the OD600 spectrophotometrically and by counting the colony-forming units (CFU). A bacterial sample was serially diluted, and a known volume was plated either onto LB or BHI agar. The cell concentration was obtained by counting the number of colonies that had formed.

### Intracellular Metabolite Extraction by Cold Methanol (Fingerprinting)

For each bacterial culture a total amount of 50 mL was collected in the exponential phase (OD600 = 0.6) on separate 0.22 µm filters.<sup>27</sup> Immediately after the disappearance of the culture medium the unwashed filters were transferred to liquid nitrogen. Subsequently each filter was crushed into separate conical tubes and was suspended in 5 mL of 100% cold methanol which was cooled to below -40 °C in a dry ice-ethanol bath. Three freeze-thaw cycles were applied to break the cell wall and to release the intracellular metabolites. The lysates were centrifuged at 4000g for 15 min at 4 °C, and the supernatants were transferred into a clean tube. The metabolites were purified by adding 5 mL of water and 10 mL of chloroform and shaking for 5 min. The water-methanol phase contained the metabolites and was separated from the lipophilic chloroform-phase by centrifugation for 15 min at 4000g. The metabolite solution was transferred to a clean tube, and 1 mL was aliquoted into 1.5 mL tubes 3×. The samples were dried in a speed-vacuum evaporator, resuspended in 500 µL of D<sub>2</sub>O, and stored at -20 °C.

### Bacterial Culture Growth Medium (Footprinting)

Samples for footprinting were prepared simultaneously with intracellular metabolite extraction. After bacterial cells were separated by filtration, the filtrate was stored at -20 °C until the NMR measurements were performed.

### Mice

Experiments were performed on 5 to 8 weeks-old (20–35 g) male mice. TLR4-/ mice and C57BL/6 mice were purchased from The Jackson Laboratory (Bar Harbor, ME). TLR2-/ mice were provided by Prof. Shizuo Akira (Osaka University, Japan). Mice were maintained in a pathogen-free environment. The mice had access to food and water *ad libitum*. All procedures performed were approved by the University of Calgary Animal Care Committee and were in accordance with the Canadian Guidelines for Animal Research.

## Induction of Bacterial Infections in Mice

Bacterial cultures in the exponential phase (see Bacteria and Growth Conditions) were centrifuged for 10 min at 3000 rpm and washed twice with saline, and the cell concentration of the bacterial suspension was adjusted by spectrophotometry at 600 nm. To induce the different bacterial infections in mice, animals were injected intraperitoneally with 1 mL of the bacterial suspensions adjusted to the following concentrations: *S. aureus*:  $1 \times 10^7$  CFU/mL; *S. pneumoniae*:  $1 \times 10^7$  CFU/mL; *P. aeruginosa*:  $1 \times 10^6$  CFU/mL; *E. coli*:  $1 \times 10^7$  CFU/mL. For *P. aeruginosa* concentrations of  $7 \times 10^2$  CFU/ml,  $8 \times 10^4$  CFU/mL and  $5 \times 10^6$  CFU/mL were also investigated.

## Treatment of Mice with LPS and MALP2

MALP2 and LPS (LPS from *Escherichia coli* O111:B4) were purchased from Alexis Biochemicals (Enzo Life Sciences, Inc., Plymouth Meeting, PA) and List Biologicals (Burlington, Ontario, Canada), respectively. MALP2 (5 µg) was dissolved in 200 µL of saline and intraperitoneally injected into wild-type and TLR2-/ mice. For the corresponding LPS experiment, 200 µL of saline containing 0.5 mg of LPS/kg mouse were administered in wild-type and TLR4-/ mice. Control mice received 200 µL of saline ip.

## Physiological Parameters

**Weight.** Prior to administration of bacteria, LPS, MALP2 or saline and 24 h post administration, body weight (Metler Toledo, Columbus, OH) was determined and calculated as weight loss normalized to the primary body weight.

**White Blood Cell Count (WBC Count).** Twenty-four hours after treatment and infection, mice were anesthetized by inhalation with isoflurane (Bimeda-MTC, Cambridge, Ontario, Canada), and 500 µL of blood was collected via cardiac puncture. Circulating leukocyte counts were determined with a Bright-line hemocytometer (Hausser Scientific, Horsham, PA). Blood smears were stained with Wright-Giemsa (VWR, Edmonton, Alberta, Canada) and leukocyte differentials determined from a count of 100 cells. The remaining blood volume was allowed to sit at room temperature for 10-30 min to clot and spun down at 5000 rpm for 10 min, and the top layer of serum was collected and frozen at -20 °C to be used later for metabolite and cytokine measurements.

**Peritoneal Lavage.** After the collection of blood, mice were sacrificed, and a peritoneal lavage was performed using 3 mL of warm saline. The exudate was recovered following a 60 s gentle manual massage, and leukocytes were counted with a hemocytometer.

**Myeloperoxidase (MPO) Activity.** From sacrificed mice, lung tissue was collected and used for an MPO activity assay. MPO is a myeloid cell-specific enzyme in neutrophils, and its activity was measured to determine the neutrophil influx into the lung.<sup>28,29</sup> Lung tissues were prepared in 96-well plates and processed using hexadecyltrimethylammonium bromide (for enzyme extraction) and dianisidine-H<sub>2</sub>O<sub>2</sub> (as the colorimetric substrate) (Sigma, St. Louis, MO). The assay was performed following a previously published protocol.<sup>30</sup> The change in absorbance at 450 nm in the 96-well plates was determined over 60 s using a kinetic microplate reader (Molecular Devices, Sunnyvale, CA).

**Lung CFU.** At 24 h after inoculation mice were sacrificed and lungs were collected and homogenized in 1 mL of sterile PBS. Bacterial CFU were determined by culturing serial dilutions on LB agar plates overnight at 37 °C.

**Chemokines and Cytokines.** The analysis of the cytokines and chemokines in mouse serum was performed with a BioPlex 8 plex immune assay kit (IL-6, IL-10, G-CSF, KC, MCP-1, MIP-1 $\alpha$ , RANTES, TNF $\alpha$ ) from BioRad (Herkules, CA) according to the manufacturer's specifications. The plate was read on a Luminex 200 apparatus (Applied Cytometry Systems, UK). The acquisition and analysis were performed with the STarStation V.2.3 software from Applied Cytometry Systems.

## NMR Sample Preparation

All of the serum samples from mice as well as the samples for footprint and fingerprint-analysis were filtered in 3-kDa-cutoff spin columns (3 K Nanosep: Omega; VWR, Edmonton, Alberta, Canada), and filtered protein was rinsed using an additional 100 µL of D<sub>2</sub>O. Prior to use, filters were washed 5 times with water and then D<sub>2</sub>O to remove the glycerol conservation agent. The final sample volume ranged from 300 to 500 µL and was transferred to clean microfuge tubes. Samples were brought to a total volume of 650 µL by addition of D<sub>2</sub>O, 40 µL of sodium azide (1 M NaN<sub>3</sub> solution), and 140 µL of phosphate buffer (500 mM NaH<sub>2</sub>PO<sub>4</sub> buffer solution at pH 7.0) containing 2.5 mM of 2,2-dimethyl-2-silapentane-5-sulfonate (DSS) as an internal chemical shift and concentration standard, and the pH was adjusted to 7.00 ± 0.05.<sup>12,31,32</sup>

## NMR Acquisition

All NMR experiments were acquired on a Bruker AVANCE 600 spectrometer equipped with a 5 mm TXI probe (Bruker, Milton, Ontario, Canada) at 298 K. The 1D <sup>1</sup>H NMR spectra were obtained using a standard Bruker 1D nuclear Overhauser enhancement spectroscopy (NOESY)-presaturation pulse sequence (noesypr1d)<sup>13,33</sup> in which the residual water peak was irradiated during the relaxation delay of 1.0 s and during the mixing time of 100 ms. For an overall recycle time of 5 s an acquisition time of 2 s and an initial relaxation delay of 3 s was used. A total of 2048 and 1024 scans were collected for samples of mouse serum and culture experiments, respectively. All spectra were acquired, zero filled to 64k points and Fourier transformed. The spectra were manually corrected for phase and baseline distortions within Topspin (Bruker Biospin, Ltd.) and were referenced to the DSS resonance at 0.0 ppm. Additional two-dimensional NMR experiments such as total correlation spectroscopy (2D <sup>1</sup>H-<sup>13</sup>C TOCSY) and heteronuclear single quantum coherence spectroscopy (2D <sup>1</sup>H-<sup>13</sup>C HSQC) were performed for chemical shift assignments and verification.

## Targeted Metabolite Profiling

1D <sup>1</sup>H NMR spectra were imported into Chenomx NMR Suite version 4.6 (Chenomx Inc., Edmonton, Canada) for metabolite identification and quantification by targeted metabolite profiling analysis in the Profiler module which is linked to a library representing over 260 metabolite entries.<sup>13</sup> To determine the concentration of individual compounds the concentration of DSS was used as reference. Each compound concentration was then normalized to the sum of all concentrations, excluding the two highest concentrated metabolites, glucose and lactate, which otherwise would dominate the normalization.<sup>34</sup> These normalized data were then used for multivariate statistical data analysis. A total of 43 metabolites were profiled in serum spectra. For the fingerprint and footprint spectra 39 metabolites were identified.

## Multivariate Data Analysis

The final data set used for the multivariate analysis consisted of eight wild-type C57BL/6 mice for each bacterial infection (*S. aureus*, *S. pneumoniae*, *E. coli*, *P. aeruginosa*), eight wild-type mice with LPS injection, seven wild-type mice with saline, and six mice with MALP2 treatment. Four TLR4<sup>-/-</sup> mice were injected with either *E. coli* or LPS, and four TLR2<sup>-/-</sup> mice were infected with *S. aureus* and treated with MALP2, respectively. For control experiments, four saline-treated knockout mice were used for each group. For foot- and fingerprint analysis, six samples per bacterial strain were prepared, respectively, using two biological duplicates. Chemometric analysis was performed using SIMCA-P version 11.5 (Umetrics, Umea, Sweden) and both supervised (partial least-squares, partial least-squares discriminant analysis, orthogonal partial least-squares discriminant analysis), and unsupervised (principle component analysis) projection techniques were applied to the different data sets.

PCA models were applied to each treatment-control data set as well as to all serum samples collected from *S. aureus*, *S. pneumoniae*, *E. coli*, and *P. aeruginosa* infected mice. As an unsupervised method, PCA defines the major sources of variance without over interpretation and allows outliers to be identified.<sup>14</sup> To reveal differences in the metabolomic profiles which may be masked by PCA using all data points, supervised PLS-DA modeling was applied using a binary variable as class-membership for different bacterial infections and treatments.

By OPLS-DA an orthogonal projection was conducted for each individual bacteria-host and footprint-medium data set. However these supervised models may also contain variation that is not class-related and which can be avoided applying PLS analysis to the <sup>1</sup>H NMR spectral information with additional orthogonal class-characteristics. Here we conducted PLS analysis using a metabolomic matrix x and an identity-matched matrix y containing a set of physiological-immunological data in order to find connections between the two sets of data. In our calculations, we used a total loadings set consisting of eight physiological (weight, WBC counts, lymphocytes, monocytes, neutrophiles, eosinophiles, MPO, leukocytes in peritoneal lavage), eight immunological parameters (IL-6, IL-10, G-CSF, KC, MCP-1, MIP-1 $\alpha$ , RANTES, TNF $\alpha$ ), and 43 quantified metabolites. The quality of each model was assessed by the parameters R<sub>2</sub> and Q<sub>2</sub>. R<sub>2</sub> is the goodness-of-fit parameter, the percentage of variation explained in the data, and Q<sub>2</sub> the goodness of prediction parameter based on a 7-fold cross validation approach.<sup>35</sup>

## RESULTS

### Validation of the Mouse Model for Different Bacterial Infections

To establish a reliable mouse model, *S. aureus* infections were induced with the bioluminescence Xen29 strain in wild-type C57BL/6 mice by intraperitoneal (ip,  $1 \times 10^7$  CFUs), intravenous (iv,  $1 \times 10^7$  CFUs), and subcutaneous (sc,  $1 \times 10^8$  CFUs) administration. Their progression was monitored by bioluminescence as well as by NMR-based metabolomics. Over the course of 24 h, the intensity of the bioluminescence changed significantly when following the concentration of detectable pathogens located closely to the skin surface (Figure 1A). The fast systemic distribution of bacteria after intraperitoneal invasion led to a loss in intensity after 24 h compared to 4 h, while for the subcutaneous injection both an increase in

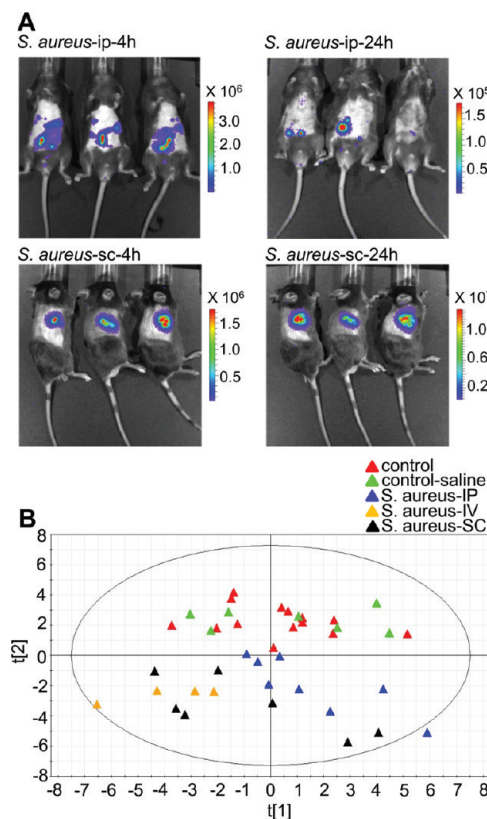


**Figure 1.** Comparison of intravenous (iv), intraperitoneal (ip), and subcutaneous (sc) administration of *S. aureus*. (A) *S. aureus* Xen29 possessing a stable copy of the luxABCDE operon was imaged to study the redistribution of bacteria after ip and sc injection. Images obtained after 4 and 24 h are shown. While there appears to be little redistribution from the initial injection site after sc injection, good redistribution is observed following ip injection. (B) PCA analysis (three components,  $R^2 = 0.48$ ,  $Q^2 = 0.25$ ) of serum of *S. aureus* infected mice and controls. The analysis shows that the three routes of administration (sc, ip, iv) give comparable results when compared against control mice and mice injected with saline. In particular, ip and sc administration show good agreement with each other. Nontreated mice and saline injected mice behaved in a very similar manner.

bacterial density as well as an expanded infected skin area developed. Because of immediate dispersion in blood after intravenous administration, much of the bacteria was rapidly cleared and no bioluminescence signal could be detected in these mice after 4 or 24 h. After bioluminescence monitoring, serum was collected by cardiac puncture, and 43 metabolites were identified and quantified by <sup>1</sup>H NMR and compared with those detected in controls (untreated,  $n = 14$ ; sham infected with 1 mL of saline ip injected,  $n = 7$ ) using multivariate statistical pattern recognition techniques. Principle component analysis (PCA; three components,  $R^2 = 0.48$ ,  $Q^2 = 0.25$ ) scores plots revealed complete class distinction in the second component between infected and healthy subjects (Figure 1B). No separation was observed between untreated animals and those having received an ip injection of 1 mL saline. However in the group of the infected subjects, serum samples of infected mice having the same site of infection grouped together in the first component according to the similarities in their metabolomic profiles. Additionally, CFU counts in lung tissue confirmed reliable systemic progression of the infection for both the intraperitoneal and intravenous routes of administration. Since ip invasion of bacteria is one of the

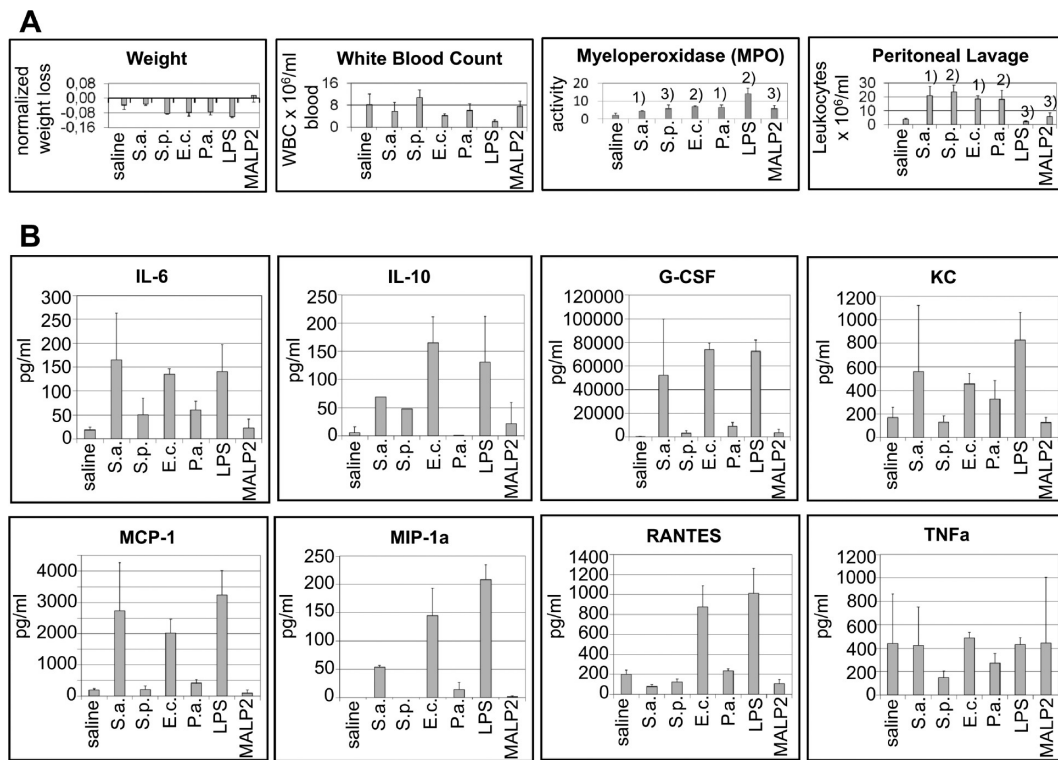


**Figure 2.** Physiological and immunological conditions in response to bacterial infections and to LPS and MALP2 administration, 24 h post-infection. C57BL/6 wild-type mice were infected intraperitoneally with 1 mL of *S. aureus* (S.a.), *S. pneumoniae* (S.p.), *E. coli* (E.c.), and *P. aeruginosa* (P.a.) suspensions. Saline, LPS, and MALP2 were also ip-injected. (A) Weight loss, MPO activity from lung tissue and leukocyte counts from both blood and peritoneal lavage. Significance of paired *t* tests on differences in physiological parameters between controls and infected mice (1)  $p < 0.01$ , (2)  $p < 0.002$ , (3)  $p < 0.05$ . White blood cell counts did not differ significantly between the control group and infected mice. (B) Levels of cytokines and chemokines in mouse serum.

more clinically relevant routes of infection leading to life threatening septicemic conditions in patients, the ip infection model was utilized for all further investigations.

In our study, we investigated host-microbe interactions using two Gram-positive and two Gram-negative organisms: *S. aureus*, *S. pneumoniae*, *E. coli*, and *P. aeruginosa*. The bacterial dose was adjusted to  $10^7$  CFU/mL for *S. aureus*, *S. pneumoniae*, and *E. coli* and  $10^6$  CFU/mL for *P. aeruginosa* and resulted in a survival rate of 100% on day one post injection. Twenty-four hours post bacteria administration, mice ( $n = 8$  for each kind of infection) showed CFUs in the lungs (results not shown) as a result of a systemic progression of the bacterial infection. Additionally, mice were examined according to their health condition and status of inflammation by comparing body weight, Myeloperoxidase (MPO) activity in the lungs, white blood cell counts in blood and peritoneal lavage, as well as cytokine/chemokine levels (IL-6, IL-10, G-CSF, KC, MCP-1, MIP-1 $\alpha$ , RANTES, TNFa) in serum (Figure 2). The data were compared with sham mice (ip injection of 1 mL of saline,  $n = 7$ ) and animals having obtained an intraperitoneal injection of LPS ( $n = 8$ ) and MALP2 ( $n = 6$ ). For LPS and MALP2, a dose of 0.5 mg/kg and 5  $\mu\text{g}/\text{mouse}$  dissolved in a volume of 200  $\mu\text{L}$  saline was applied, respectively. Twenty-four h after infection, some animals showed signs of diarrhea and stopped eating and drinking, which resulted in a higher weight loss compared to the control group (Figure 2A). All infected mice developed to a similar extent significantly elevated leukocyte counts in the peritoneal lavage ( $p < 0.01$ ) as well as increased MPO activity ( $p < 0.05$ ) in the lungs as a result of neutrophilic influx while white blood counts in blood did not change significantly compared to the

controls. In addition, animals showed enhanced serum levels of different cytokines (IL-6, IL-10, G-CSF, and TNFa) and chemokines (KC, MCP-1, MIP-1 $\alpha$ , RANTES) demonstrating that an intense systemic inflammatory response has developed (Figure 2B). Extremely high cytokine and chemokine concentrations were found for *S. aureus* and *E. coli* infections and for mice having been treated with LPS. Taken together, these data show that in all cases a systemic infection was obtained. Although the responses did vary in magnitude with *S. aureus* and *E. coli* having the highest responses, the responses for all bacteria, LPS and MALP2 were elevated in a similar direction.

#### Metabolic Similarities and Differences between *E. coli*, *P. aeruginosa*, *S. aureus*, and *S. pneumoniae* infections

To determine whether the metabolomic profiles of different infections were sufficiently unique to facilitate the identification of bacteria specific biomarkers, supervised multivariate statistical modeling was applied to a set of 43 identified serum metabolites obtained from *S. aureus*, *S. pneumoniae*, *E. coli* and *P. aeruginosa* infected mice. Metabolites that were identified included several intermediates of the tricarboxylic acid (TCA) cycle, glycolysis, as well as fermentation and lipid precursor metabolites. In addition, ketone bodies, amino acids, as well as carboxylic acids which were caused by direct cellular events were detected. Some metabolites such as taurine are related to the innate immune system and released by the polymorphonuclear cells, while others derive from bacteria in the gut and at the site of infection. A full list of metabolites and

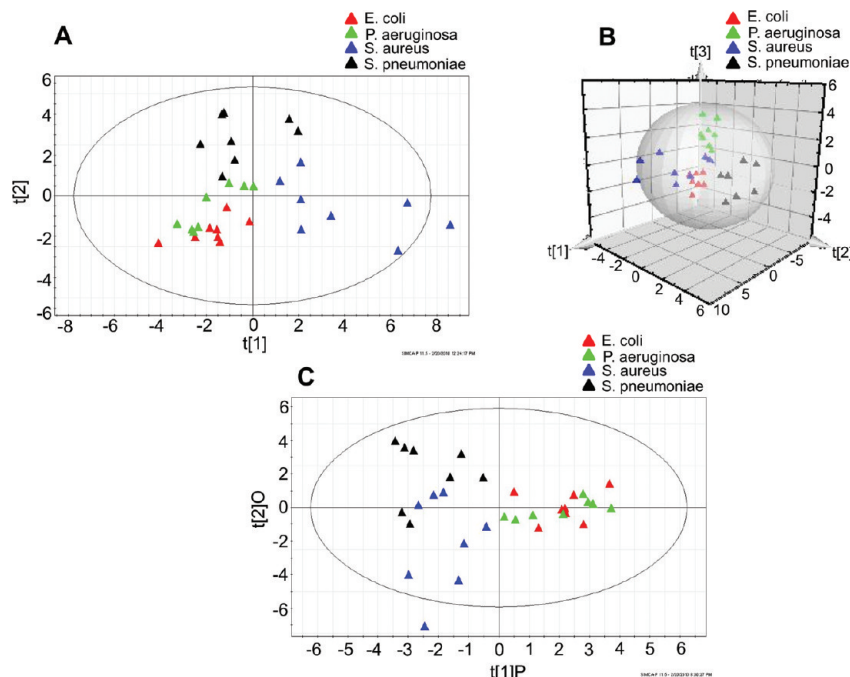


**Figure 3.** Scores plots representing  $^1\text{H}$  NMR spectral data from serum of C57BL/6 wild-type mice infected with four different bacterial strains. Mice were infected intraperitoneally with 1 mL of *S. aureus* (*S.a.*), *S. pneumoniae* (*S.p.*), *E. coli* (*E.c.*), and *P. aeruginosa* (*P.a.*) suspensions, and serum was analyzed 24 h post administration. (A) 2D and (B) 3D PLS-DA scores plots (based on 43 metabolites) showing differentiation between the four bacterially infected mouse models (three components;  $R^2 = 0.71$ ,  $Q^2 = 0.56$ ). The 3D plot represents similarities along the third principle component for *E. coli* and *P. aeruginosa* infected groups and along the  $x^2 - y^2$  axis for *S. aureus* and *S. pneumoniae* infections. (C) OPLS-DA scores plot separating the samples of Gram-positive (*S. aureus*, *S. pneumoniae*) and Gram-negative (*E. coli*, *P. aeruginosa*) infections (two components;  $R^2 = 0.81$ ,  $Q^2 = 0.59$ ).

their biological relevance is summarized in Table 1 of the Supporting Information.

Using PLS-DA, a clear separation between the four bacterial strains was obtained (Figure 3A). Three components of the PLS-DA analysis encapsulated 71% of the interclass variation ( $R^2$ ) with a corresponding cross-validation accuracy of 56% ( $Q^2$ ). Coefficients of metabolites for different bacterial infections showed that each infection was correlated to specific changes in certain metabolic intermediates (Table 2A–D, Supporting Information). Mice infected with *S. aureus* showed extremely enhanced serum levels of metabolites related to fatty acid oxidation such as acetone, 3-hydroxybutyrate, and 2-hydroxybutyrate as well as isobutyrate and creatine. In contrast, in *S. pneumoniae* infections these metabolites were identified as negative contributors, and TCA cycle intermediates (2-oxoglutarate, citrate, and fumarate) as well as glucose and pyruvate showed the highest serum levels compared to all infections investigated. Hippurate, a carboxylic acid and endogenous conjugate which is not further metabolized but actively secreted by tubular cells and excreted in urine,<sup>36</sup> became a metabolite of special interest as its serum concentrations rose by almost 100% during the pneumococcal infection. It is produced by condensation of benzoic acid and glycine in the mitochondria of liver and kidney,<sup>37,38</sup> and its synthesis is stimulated by metabolic acidosis. It belongs to the group of uremic toxins, and its enhancement in urine is often used as an indicator of intrahepatic tracer dilution to determine the activity of specific human enzymes.<sup>39,40</sup> Therefore, unlike the cytokines and chemokines which simply indicated indiscriminate inflammation, metabolites highlighted striking differences.

As for the Gram-negative bacterial strains, the distinction between the metabolic profiles of *E. coli* and *P. aeruginosa* infections was mainly based on changes in amino acid blood levels, whereas varying concentration changes of energy metabolites were observed.

Besides significant distinction between different bacterial infections, similarities also became obvious in the 3D PLS-DA scores plot (Figure 3B). The clustering of *S. aureus* and *S. pneumoniae* infected mice showed similar metabolite changes in the third principal component while similar values for the first and second principal component along the  $x^2 - y^2$  axis, were obtained for *E. coli* and *P. aeruginosa* infections. Using the supervised OPLS-DA (orthogonal partial least-squares discriminant analysis; two components,  $R^2 = 0.81$ ,  $Q^2 = 0.59$ ) analysis (Figure 3C), serum samples of mice infected with Gram-positive and Gram-negative bacteria clustered as two separate groups. Five of 10 metabolites that were identified as significant positive contributors in the class of Gram-positive bacterial infections (Table 2E, Supporting Information) were glycolysis and TCA cycle intermediates such as glucose, pyruvate, citrate, fumarate, and 2-oxoglutarate. Amino acids, in contrast, were found in higher levels in blood of mice infected with Gram-negative bacteria.

Taken together, these results demonstrate that different bacterial infections give rise to individual metabolomic profiles with overlapping similarities in metabolite classes according to their gram nature.

#### Correlation between Bacteria Specific Metabolites in Vivo and the Intra- and Extracellular Bacterial Metabolomes

To investigate whether some of the metabolites which were identified as positive contributors for *S. aureus*, *S. pneumoniae*,

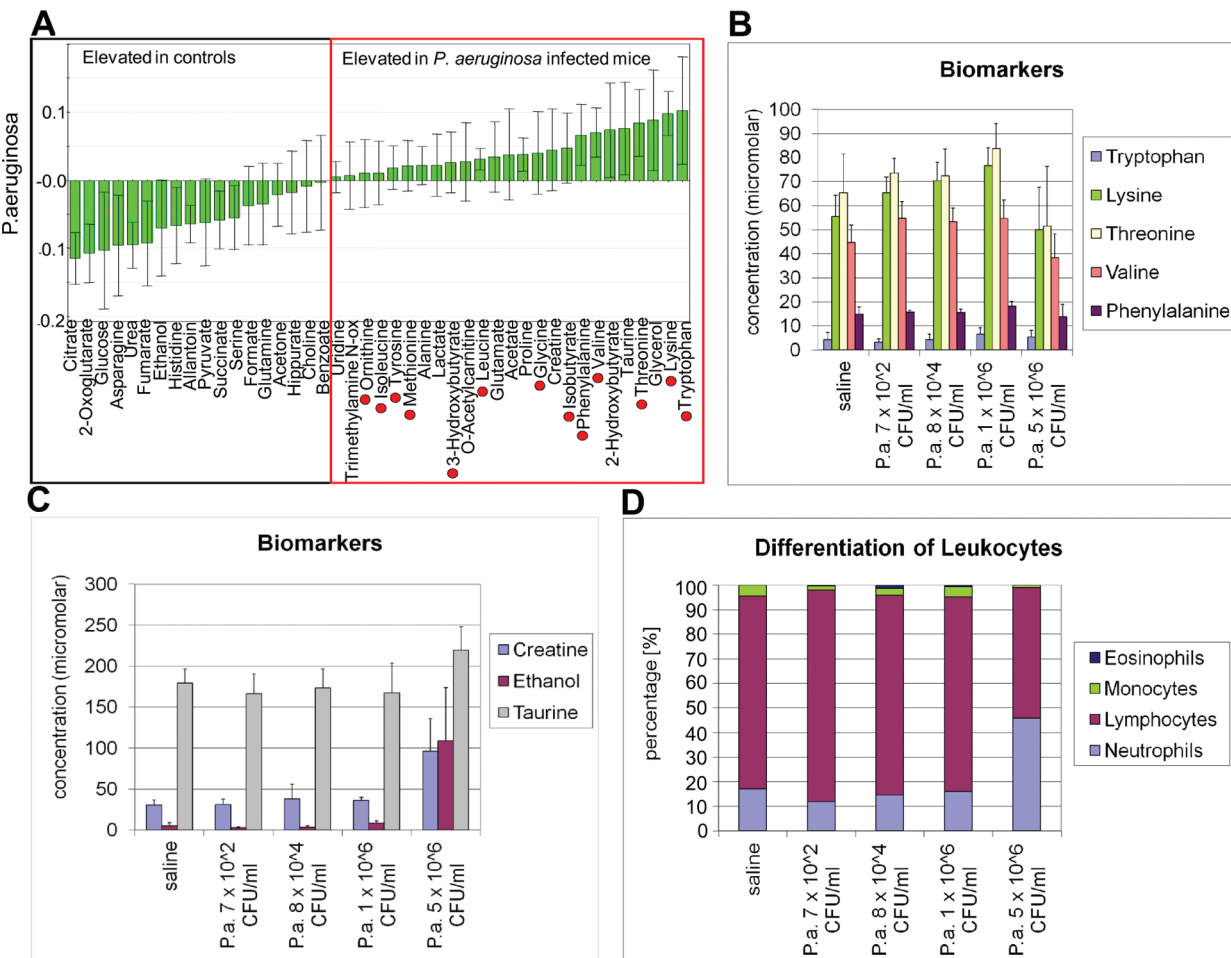


**Figure 4.** Bacterial exometabolome and metabolic host response to *P. aeruginosa* infected C57BL/6 wild-type mice 24 h post-infection. Some of the elevated serum metabolites of *P. aeruginosa* infected mice were identified as part of the bacterial exometabolome. (A) Coefficient plot generated from OPLS-DA analysis of the samples from the *P. aeruginosa* mouse model and control animals representing the relative contribution that each metabolite makes to the distinction between the two classes (two components;  $R^2 = 1.00$ ,  $Q^2 = 0.99$ ). Highlighted metabolites (red circles) were elevated both in serum samples of infected mice and in the footprints of *P. aeruginosa* cultures grown in LB medium. Tryptophan, lysine, threonine, valine, and phenylalanine were significantly elevated both in vivo and in the bacterial culture media ( $p < 0.05$ ). (B) Metabolite levels of tryptophan, lysine, threonine, valine, and phenylalanine found in serum of mice infected with *P. aeruginosa* concentrations of  $7 \times 10^2$ ,  $8 \times 10^4$ ,  $1 \times 10^6$ , and  $5 \times 10^6$  CFU/mL. Bar charts showing (C) metabolite levels of taurine, ethanol, and creatine and (D) blood leukocyte counts from serum of *P. aeruginosa* infected mice as a function of different bacterial concentrations.

*E. coli*, and *P. aeruginosa* infections in vivo were derived directly from bacterial metabolism, we conducted in vivo experiments with bacterial cell cultures. By metabolic footprinting (extracellular bacterial metabolites released into the culture medium) and fingerprinting (intracellular metabolites, extracted by organic solvents) we defined the pattern of extra- and intracellular bacterial metabolites, respectively. In our experiments, bacteria were cultured to an OD<sub>600</sub> of 0.6 in either LB (*S. aureus*, *P. aeruginosa*, *E. coli*) or BHI (*S. pneumoniae*) medium and were separated subsequently using the filtration method (0.2  $\mu$ m). Intracellular metabolites were extracted by cold methanol, and NMR data were collected from both extracts (fingerprints) and culture media (footprints). In these spectra we identified and quantified 39 metabolites including amino acids, alcohols, and organic acids. Since cultivation of the different bacterial strains required different culture media, we compared the metabolic footprint of each pathogen directly with that of the corresponding culture medium using OPLS-DA. In *S. pneumoniae*, *S. aureus*, and *E. coli* cultures, metabolite levels linked to pathways of energy supply

increased significantly during cell growth, while most of the amino acid concentrations decreased and were taken up by the bacteria to be used for protein, DNA/RNA, and cell wall synthesis.

For *P. aeruginosa*, in contrast, metabolomic footprints displayed increased concentrations for a variety of different amino acids, while positive contributors derived from anaerobic or aerobic energy metabolism were not discovered. A comparison of the metabolic profiles with those from serum of *P. aeruginosa* infected mice showed similarities for a large number of metabolites (Figure 4A), indicating that *P. aeruginosa* secretes specific metabolites which contribute directly to the serum metabolome. In subsequent experiments, *P. aeruginosa* suspensions were injected at different concentrations ( $7 \times 10^2$ ,  $8 \times 10^4$ ,  $1 \times 10^6$ ,  $5 \times 10^6$  CFU/mL) to investigate the effects of increasing bacterial load and disease stages in the mouse model. Even though MPO and leukocyte counts in the peritoneal lavage increased significantly beginning with a bacterial concentration of  $1 \times 10^6$  CFU/mL, no significant changes in WBC or severe disease symptoms as

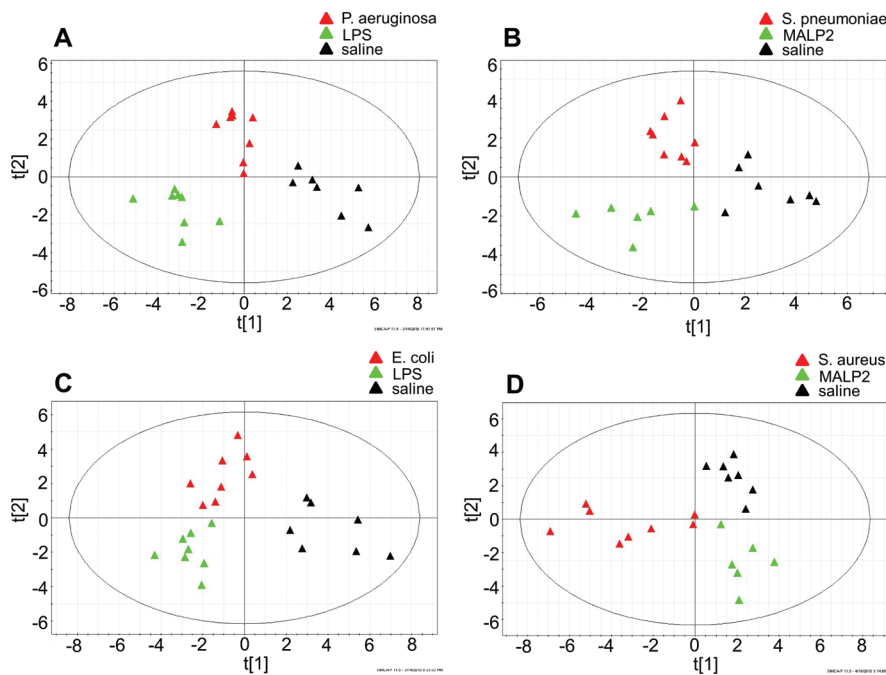


**Figure 5.** Similarities between TLR2 and TLR4 agonists and Gram-negative and Gram-positive bacterial infections. PLS-DA scores plot of serum  $^1\text{H}$  NMR data of (A) *P. aeruginosa* (three components,  $R^2 = 0.92$ ,  $Q^2 = 0.81$ ) or (C) *E. coli* (two components,  $R^2 = 0.77$ ,  $Q^2 = 0.65$ ) infected mice vs LPS treated animals and controls and (B) *S. pneumoniae* (two components,  $R^2 = 0.92$ ,  $Q^2 = 0.81$ ) or (D) *S. aureus* (two components,  $R^2 = 0.76$ ,  $Q^2 = 0.60$ ) infected mice vs MALP2 treatment and controls.

illustrated by the neutrophil-lymphocyte ratio in Figure 4D were induced for the first three bacterial concentrations. However, serum levels of the five significantly elevated metabolites tryptophan, lysine, threonine, valine, and phenylalanine continuously increased in serum with higher number of bacteria. This indicates that these metabolites may be released by the bacteria as bacterial footprints into the bodily fluids (Figure 4B). On the other hand, a more profound host response was observed when a *P. aeruginosa* suspension with a concentration of  $5 \times 10^6$  CFU/mL was applied. At 24 h post administration, these mice developed signs of severe sickness (decreased WBC, increased neutrophil-lymphocyte ratio) and also experienced decreased serum amino acid levels (Figure 4B) as well as elevated serum concentrations of ethanol, taurine, and creatine (Figure 4C) and a mortality rate of 50%.

For *E. coli*, *S. aureus*, and *S. pneumoniae* infected mice the similarities between the *in vivo* experiments and the bacterial culture footprint experiments were less distinctive. For *E. coli* and *S. aureus* only ethanol and acetone were found as secreted metabolites, while for *S. pneumoniae*, none of the increased serum and footprint compounds overlapped.

Fingerprint analysis by PLS-DA (three components,  $R^2 = 0.98$ ,  $Q^2 = 0.98$ ) showed clear separation between all four bacterial strains with differences in amino acid levels, energy metabolites as well as organic acids. However the metabolites found intracellularly in the bacterial cultures did not correlate with any metabolites found in the serum of the infected mice.

#### Characterization of the Effects of Virulence Factors in the Host

In order to distinguish between bacteria and host responses we injected mice with LPS or MALP2 to activate different TLRs. The advantage of using LPS over intact bacteria is that it should elicit a host response for a Gram-negative organism but does not contribute bacterial metabolites. Likewise, MALP2

emulates a host response for Gram-positive bacteria. Separate PLS-DA models were constructed comparing infected, non-infected and either LPS or MALP2 treated mice. The corresponding scores plots showed well separated clusters of differently treated mice but also demonstrated similar trends for groups exposed to similar cell constituents (Figure 5). Gram-negative infected mice and animals having received LPS clustered together and were clearly separated from controls along the first component. However the *E. coli* and *P. aeruginosa* induced infections gave rise to an additional shift in the second principal component, compared to LPS treatment. In multivariate statistical modeling, the first component explains the largest source of variance in the data set, while subsequent components are orthogonal to each other and explain lower levels of data variance. Clearly, the TLR-mediated response provides the major source of variance in the case of Gram-negative bacteria. Very similar results were obtained for the comparison of the *S. pneumoniae* infected mice and those treated with the synthetic TLR2 agonist MALP2. In contrast, the *S. aureus* infected and MALP2 treated groups displayed significant differences along the first component. Compared to controls, *S. aureus* infected mice showed clear discrimination both along the first and second component while the MALP2 treated animals differed from the controls only along the second component. While activation by LPS is obviously the most important virulence factor for *E. coli* and *P. aeruginosa* infections, for *S. aureus* it appears that most of the metabolic changes are not related to a MALP2-induced host response.

#### Correlation between Metabolite Profiles and Toll-Signaling Pathways

The putative signaling receptors for LPS and MALP2 are TLR4 and TLR2, respectively. To identify specific metabolites which increase in response to the activation of the TLR4 and TLR2 receptors, we studied knockout mice. We first compared serum

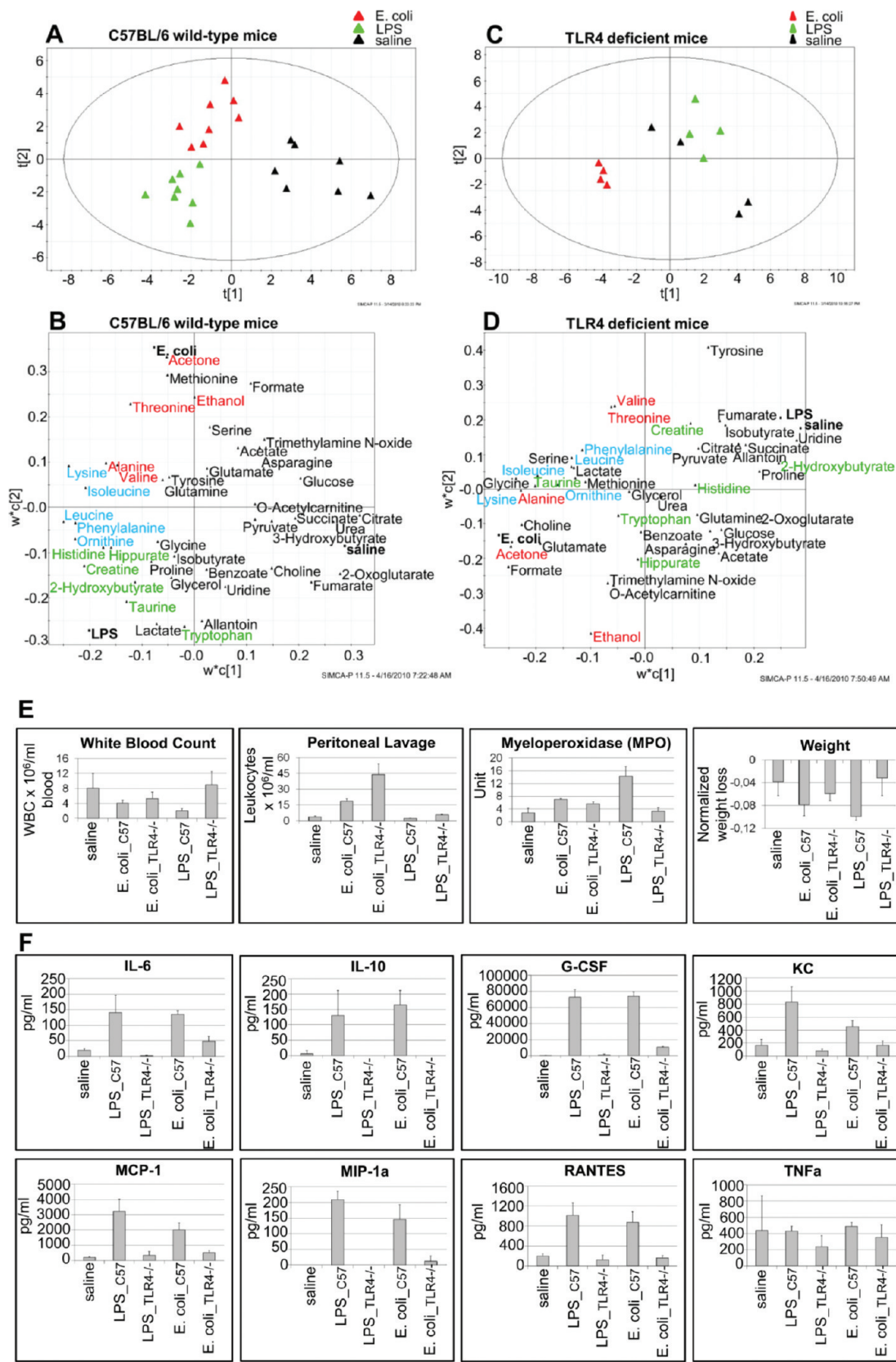


**Figure 6.** Physiological response and the metabolites and cytokines activated by the TLR4 receptor and associated signaling pathway. (A) + (B) PLS-DA modeling of metabolite concentrations identified in serum of C57BL/6 wild-type (two components,  $R^2 = 0.76$ ,  $Q^2 = 0.60$ ) and in (C) + (D) TLR4 deficient mice (two components,  $R^2 = 0.91$ ,  $Q^2 = 0.70$ ) 24 h after LPS treatment and *E. coli* infection. (A) and (C) represent scores plots from the PLS-DA analysis and (B) and (D) the corresponding loadings plots. Metabolites which were significantly enhanced in response to both LPS treatment and *E. coli* infection are highlighted in blue, those specific for LPS or *E. coli* are highlighted in green and red, respectively. In addition

Figure 6. continued

to metabolic profiles the subsequent panels show (E) leukocyte counts in blood and peritoneal lavage, MPO activity, weight loss as well as (F) cytokine and chemokine concentrations in the serum.

metabolite profiles of noninfected, *E. coli* infected and LPS treated animals both in C57BL/6 wild-type (two components,  $R^2 = 0.76$ ,  $Q^2 = 0.60$ ) and TLR4-deficient mice (two components,  $R^2 = 0.91$ ,  $Q^2 = 0.70$ ) using PLS-DA models (Figure 6). The corresponding loading plots in Figure 6 B and D give an overview of the metabolites causing the observed clustering. As shown in the previous section, in the wild-type mouse both *E. coli* infected and LPS treated animals showed similar changes in their metabolite profiles compared to controls, although they also differed from each other along the second principal component. In order to distinguish between metabolites which increased in response to an *E. coli* infection or to LPS treatment and those which were elevated in both groups, we compared each group with control animals separately via OPLS-DA. Ethanol, acetone, alanine, valine, and threonine (highlighted in red) showed substantially higher serum levels in *E. coli* infected mice than in controls, whereas the serum concentrations of creatine, hippurate, histidine, 2-hydroxybutyrate, taurine, and tryptophan (highlighted in green) were significantly elevated in the LPS group. Both disease initiators gave rise to a strong immune response and severe disease symptoms (Figure 6 E and F) and resulted in similar serum levels of lysine, leucine, isoleucine, ornithine, and phenylalanine in wild-type mice (highlighted in blue). In contrast in TLR4-deficient mice, cytokine responses and disease parameters were completely attenuated in the LPS group and strongly suppressed in infected mice identifying the TLR4 signaling pathway as major host response for *E. coli* infections. In the LPS group, normal serum concentrations were obtained similar to controls. Indeed the PLS-DA scores plot of the serum samples obtained from TLR4 deficient mice revealed only two clusters without any distinction between the control and LPS group (Figure 6C). Encouragingly, wild-type and TLR4 deficient mice respond in a similar manner to *E. coli* as evidenced by the fact that several of the induced metabolites are similar. Corresponding experiments were performed for *S. aureus* infected mice. The metabolite profiles in wild-type (Figure 7 A and B) and TLR2-deficient (Figure 7 C and D) mice were compared with those of controls as well as with MALP2 treated mice. In the loadings plot, we identified metabolites in serum of wild-type mice which were specifically elevated by the *S. aureus* infection (glycerol, creatine, acetone; highlighted red), compounds which were strongly elevated in response to MALP2 treatment (taurine, lactate, valine, isoleucine; highlighted green), and those found in increased concentration in both groups (lysine, isobutyrate; highlighted blue).

Similar to the *E. coli* and LPS experiments, described above, the class distinction between all three groups observed in wild-type mice was eliminated in TLR2 knockout mice and only metabolite profiles of mice with the *S. aureus* infection differed from those of the controls. Cytokine screening and blood cell analysis (Figure 7 E and F) confirmed that the TLR2-deficient mice had a reduced response to MALP2. However most of the cytokine levels remained elevated in *S. aureus* infected TLR2 knockout mice, indicating that other immune pathways are mainly activated.

## Correlations between Metabolic, Physiological, And Immunological Responses

To further investigate the covariation between metabolite levels and host response, PLS regression analysis of all four bacterial infections was performed using the physiological/immunological characteristics as  $y$  variables and metabolite concentrations as  $x$  variables (three components,  $R^2 = 0.72$ ,  $Q^2 = 0.52$ ). Several statistically significant correlations between physiological and immunological parameters and corresponding metabolite profiles could be derived (Figure 8). Besides well-known positive correlations between neutrophils and taurine<sup>41,42</sup> and weight loss and ketone bodies, correlations were also found between some cytokines and serum metabolites. For example, a positive correlation was found between IL6 and serum concentrations of acetone, formate, creatine, and 2-hydroxybutyrate. Similar positive relationships were identified for TNFa, G-CSF, and KC, while most of the cytokines and chemokines were negatively correlated with choline, glucose, as well as the TCA cycle intermediates citrate and 2-oxoglutarate.

## DISCUSSION

In this work, we used a simple intraperitoneal mouse model to study bacterial infections. One of our main interests was the comparison between the effects of Gram-positive and Gram-negative infections on the physiological, immunological, and metabolite response of the host. We selected for the study various bacterial strains of clinical significance: the Gram-positive strains *S. aureus* and *S. pneumoniae* and the Gram-negative strains *E. coli* and *P. aeruginosa*. In previous studies, the two Gram-positive bacterial strains *S. pneumoniae* and *S. aureus* have been compared in a mouse model,<sup>18</sup> and furthermore, different pneumonia infections have been investigated in patients.<sup>19</sup> To the best of our knowledge, ours is the first study to use a metabolomics approach to make a direct comparison between the effects of Gram-positive and Gram-negative bacteria. In order to establish that all four pathogenic bacteria induced a systemic infection with similar disease progression, we measured lung CFUs as well as several physiological and immunological responses. Because we were also interested in comparing the metabolic response and the cytokine response to infection, we used mouse serum as the biofluid of choice for our studies. In previous studies we have shown that the metabolomics analysis of mouse serum by quantitative proton NMR gives useful information about the onset of various diseases.<sup>12,43–46</sup> To facilitate comparisons, all mice were harvested at 24 h after infection and all parameters were measured at this time point.

Our results indicate that all four bacterially infected host mouse models (*S. aureus*, *S. pneumoniae*, *P. aeruginosa*, *E. coli*) gave rise to a distinct pathological phenotype based on the metabolite profiles, suggesting that different cellular functions may be impaired (Tables 1 and 2, Supporting Information). The significantly enhanced serum levels of metabolites that are related to fatty acid oxidation (e.g., the ketone bodies acetone and 3-hydroxybutyrate) as well as increases in 2-hydroxybutyrate, isobutyrate, and creatine, which were found in *S. aureus*

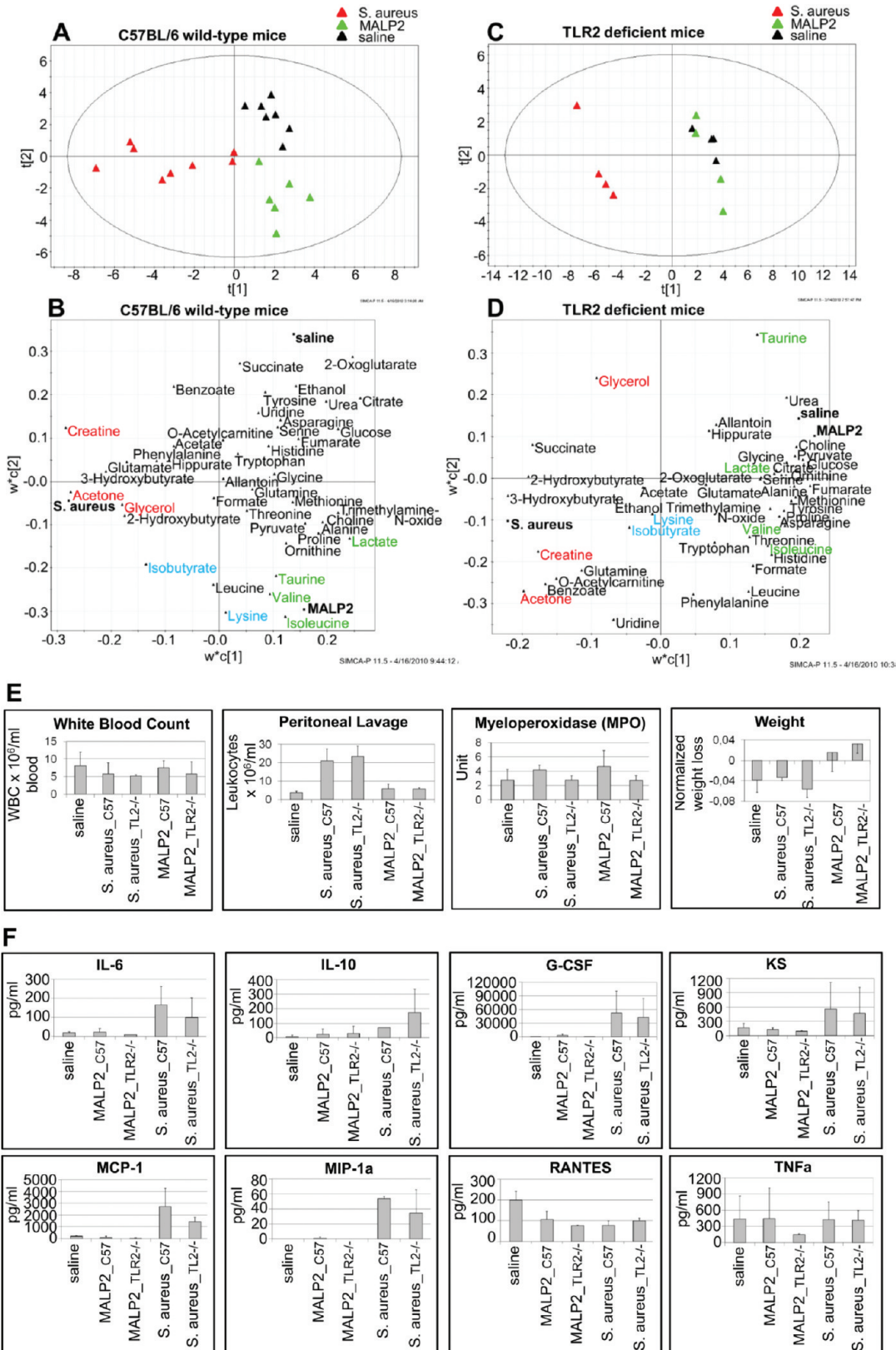


**Figure 7.** Physiological response and the metabolites and cytokines activated by the TLR2 receptor and associated signaling pathway. (A) + (B) PLS-DA modeling of metabolite concentrations identified in serum of C57BL/6 wild-type (two components, R<sub>2</sub> = 0.77, Q<sub>2</sub> = 0.65) and in (C) + (D) TLR2 deficient mice (two components, R<sub>2</sub> = 0.99, Q<sub>2</sub> = 0.97) 24 h after MALP2 treatment and *S. aureus* infection. (A) and (C) represent scores plots from the PLS-DA analysis and (B) and (D) the corresponding loadings plots. Metabolites which were significantly enhanced in response to both MALP2 treatment and *S. aureus* infection are highlighted in blue, those specific for MALP2 or *S. aureus* are highlighted in green and red, respectively. In addition to metabolic profiles, the subsequent panels show (E) leukocyte counts in blood and peritoneal lavage, MPO activity, weight loss as well as (F) cytokine and chemokine concentrations in the serum.

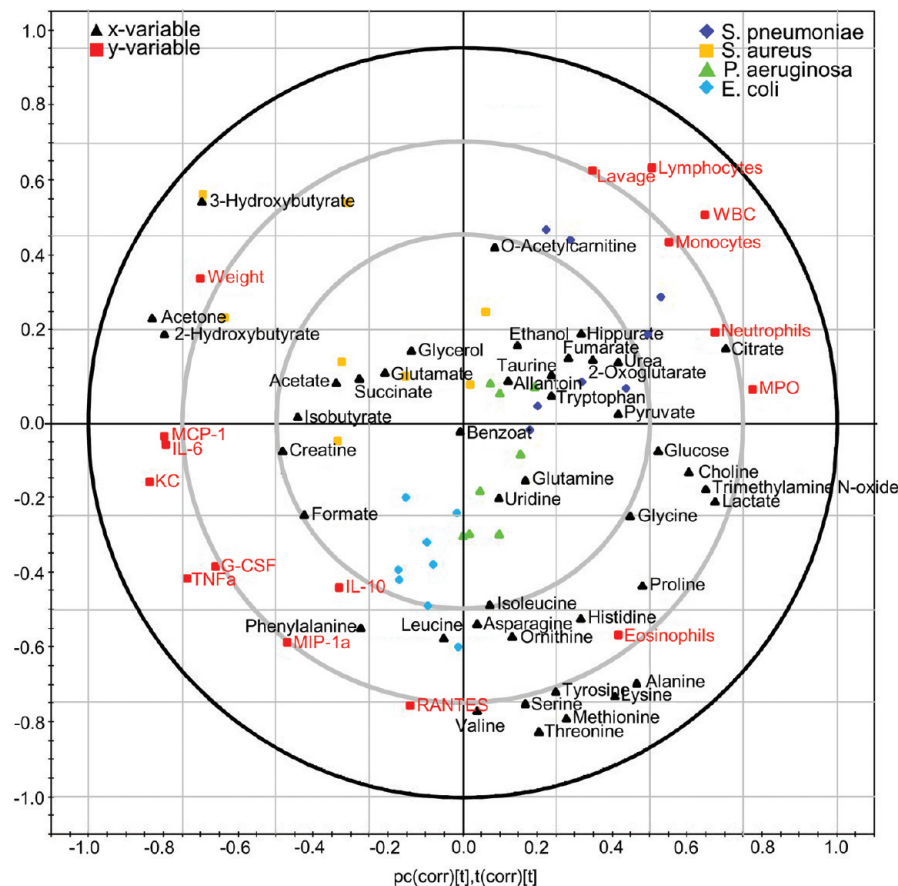


**Figure 8.** Covariation between metabolic, physiological, and cytokine responses. Correlation circle (biplot, three components,  $R^2 = 0.72$ ,  $Q^2 = 0.52$ ) of the four bacterial infections (*S. aureus*, *S. pneumoniae*, *E. coli*, *P. aeruginosa*) in C57BL/6 wild-type mice, their metabolites (*x*-variables), as well as their physiological and immunological parameters (*y*-variables).

infected wild-type mice, are indicative of severe changes in hepatic cellular functions.

In contrast, perturbations in host TCA cycle metabolites were mainly observed in *S. pneumoniae* infected mice. TCA cycle precursors and intermediates such as glucose, pyruvate, 2-oxoglutarate, citrate, and fumarate, which usually decrease in times of sickness, showed the highest serum levels in *S. pneumoniae* infected mice compared to the other bacterial infections investigated in this study. These metabolites were identified as main positive contributors in the PLS-DA model (Table 2, Supporting Information). The pyruvate concentration was even higher than in control mice. Unexpectedly high levels of 2-oxoglutarate and fumarate were also found in the urine of pneumococcal pneumonia patients.<sup>19</sup> In contrast to *S. aureus* acetone, 2-hydroxybutyrate and isobutyrate were decreased.

Overall, both Gram-positive *S. aureus* and *S. pneumoniae* infections gave rise to increased energy metabolites causing clear distinction from the Gram-negative bacterial infections in the OPLS model. With a > 50 % negative culture in septic patients, it seems imperative that an alternative approach to diagnosis is needed. Moreover, the blood cultures currently used take several days to complete, and a fast method would also be advantageous. Perhaps metabolomics can become a useful clinical tool to distinguish between Gram-positive and Gram-negative infections to better inform the physician. Although encouraging, further studies are necessary to verify and extend these initial observations.

In mice infected with Gram-negative bacteria, we observed that amino acid serum levels were strongly elevated and were partly derived from the bacterial exometabolome, particularly in the case of *P. aeruginosa* infections. The secreted metabolites identified in our bacterial culture experiments (Figure 4A) were consistent with previous reports in the literature.<sup>47</sup> However, bacterial metabolism strongly depends on culture conditions, and the lack of agreement for metabolites found *in vivo* and in cultures of *S. aureus*, *S. pneumoniae*, and *E. coli* may be caused by the different composition of blood and culture media or the oxygenation status.

Our study also demonstrated that metabolomics is a useful tool to investigate the effects of potential virulence factors and signaling pathways *in vivo*. Comparisons of the serum metabolites from mice treated with the immune stimulators LPS and MALP2 and Gram-negative and Gram-positive bacterial infections showed significant similarities (Figure 5). For example, the metabolite profiles of serum from mice infected with *E. coli* and of mice treated with LPS differed only in the metabolites such as valine, threonine, alanine, acetone, and ethanol (Figure 6). Acetone and ethanol were identified as bacterial metabolites involved in cellular energy metabolism, while the amino acids seemed to be induced by other virulence factors different from LPS.

Investigation of *E. coli* infection and LPS induced host responses in both wild-type and TLR4 deficient mice clearly identified LPS as the main virulence factor. TLR4 was verified

as the key receptor in immune stimulation by Gram-negative bacteria resulting in reduced metabolic as well as physiological and immunological responses to LPS in TLR4 deficient mice. In *E. coli* infected knockout mice in contrast, physiological and metabolic responses to the infection remained observable while their immunological response was almost completely attenuated. The same metabolites which were significantly elevated in wild-type mice were also increased in TLR4 deficient animals. This indicates a strong correlation between physiological and metabolic responses to an infection which seem to be independent from the activation of the host immune response and in this case TLR4 specifically.

In concordance with the *E. coli*/LPS experiment, the metabolic, physiological, and immunological responses to MALP2 were attenuated in TLR2-deficient mice. The same metabolites were elevated both in wild-type and TLR2 deficient mice in response to *S. aureus* infections. However similarities between *S. aureus* and MALP2 were less obvious than for *E. coli* and LPS pointing out the complexity of an *S. aureus* infection and its virulence factors. In fact, the systemic chemokine/cytokine responses to *S. aureus* were hardly diminished in the TLR2 knockout mice, indicating that other host defense signaling pathways are also involved. For *S. aureus*, a plethora of superantigens, which can induce a strong immune response with activation of T cells at picomolar concentrations, are described in the literature<sup>48</sup> and may explain the observed differences. Complement activation also is an important *S. aureus* activation system. Finally, *S. aureus* also kills host cells inducing activation of the inflamasome and the related sterile injury danger signal pathways.

Relationships between the different bacterial infections, their metabolic, as well as their immunological and physiological responses were further investigated in the biplot shown in Figure 8. These data highlight the statistical relationships between the metabolic, cytokine, and physiological responses to infections. However, it is not clear at this stage whether there is a direct mechanistic relationship between the metabolic and the cytokine responses. The observed negative correlation between cytokines and chemokines and the intermediates of energy metabolism such as glucose, citrate, and 2-oxoglutarate may simply be caused by their decreasing concentrations in times of sickness. Similar reasoning may also apply to the relationships observed between increased ketone body, creatine and formate serum levels and elevated general cytokines such as IL-6, TNF, and G-CSF as has already been discussed for cytokine and metabolic profiles seen in protozoan infections.<sup>49</sup> Interestingly, correlations between cytokine profiles and in vivo magnetic resonance imaging and spectroscopy data have also been reported.<sup>50</sup>

Other support for this notion comes from the correlation found between IL-10, MIP-1 $\alpha$ , and RANTES and the amino acids asparagine, phenylalanine, and histidine which have been identified as positive contributors to the model in *E. coli* infected mice. However, especially for *E. coli* it should be noted that cytokine and chemokine screening showed extremely high IL-10, MIP-1 $\alpha$ , and RANTES levels which may explain the observed covariation.

## CONCLUSION

Our results suggest that different bacterial strains give rise to unique NMR-based serum profiles and that it might be possible to use this approach in the future to distinguish between Gram-positive and Gram-negative infections in a clinical setting. For

some bacterial strains, as is the case for *P. aeruginosa*, it might be possible to directly identify the infecting organism because they secrete specific metabolites into the host metabolome which can be identified. The use of different knockout mice combined with the administration of specific bacterial virulence factors allowed us to dissect bacterial and host responses. Our results illustrate that this is a powerful approach that could be applied in future studies of host response to other diseases or insults. Finally, our quantitative approach allowed us to make comparisons between the metabolic and physiological and immunological responses to an infection which may lead to a better understanding of the mechanisms of pathogenesis and immunoregulation.

## ASSOCIATED CONTENT

### Supporting Information

Mouse serum metabolites identified in this study and their biological relevance (including citations for refs 51–61); bacteria-specific metabolites found in serum of *S. aureus*, *S. pneumoniae*, *E. coli* and *P. aeruginosa* infected C57BL/6 mice by PLS-DA; OPLS-DA loadings derived from Gram-positive and Gram-negative bacterial infections. This material is available free of charge via the Internet at <http://pubs.acs.org>.

## AUTHOR INFORMATION

### Corresponding Author

\*Tel: +1-403-220-6006. Fax: +1-403-289-9311. E-mail: vogel@ucalgary.ca.

### Present Address

<sup>§</sup>Department of Clinical Radiology, University Hospital Muenster, Muenster, 48149, Germany.

### Notes

The authors declare no competing financial interest.

## ACKNOWLEDGMENTS

We thank Mr. Gavin Duggan for helpful discussions regarding the statistical analysis, Mrs. Derriice Knight for organizational support, and Dr. Brent Winston and Dr. Graciella Andonegui for providing us with the *S. pneumoniae* bacterial strain. This work was supported by an operating grant from the Canadian Institutes of Health Research (to HJV Principal Investigator) and a team grant from the Alberta Innovates Health Solutions (AIHS) funded by the Alberta Heritage Foundation for Medical Research (AHFMR) (to PK Principal Investigator). V.H. was supported by a Fellowship Award from AIHS/AHFMR. P.K. holds a Scientist Award from AIHS/AHFMR as well as the Calvin, Phoebe, and Joan Snyder Chair. H.J.V. is the holder of a Scientist Award of AIHS/AHFMR.

## ABBREVIATIONS:

BHI, brain-heart infusion; CFU, colony forming unit; ip, intraperitoneal; iv, intravenous; LB, Lutria-Bertani; LPS, lipopolysaccharide; LTA, lipoteichoic acid; OD 600, optical density at 600 nm; MALP2, macrophage-activating lipopeptide-2; OPLS-DA, orthogonal partial least-squares discriminant analysis; PAMP, pathogen-associated molecular pattern; PCA, principle component analysis; PLS, partial least-squares; PLS-DA, partial least-squares discriminant analysis; sc, subcutaneous; TLR, Toll-like receptor

## ■ REFERENCES

- (1) Gootz, T. D. The global problem of antibiotic resistance. *Crit Rev Immunol.* **2010**, *30* (1), 79–93.
- (2) Kanwar, M.; Brar, N.; Khatib, R.; Fakih, M. G. Misdiagnosis of community-acquired pneumonia and inappropriate utilization of antibiotics: side effects of the 4-h antibiotic administration rule. *Chest* **2007**, *131* (6), 1865–1869.
- (3) Scheld, W. M. Maintaining fluoroquinolone class efficacy: review of influencing factors. *Emerg Infect Dis.* **2003**, *9* (1), 1–9.
- (4) Mancini, N.; Carletti, S.; Ghidoli, N.; Cichero, P.; Burioni, R.; Clementi, M. The era of molecular and other non-culture-based methods in diagnosis of sepsis. *Clin Microbiol Rev.* **2010**, *23* (1), 235–251.
- (5) Christ-Crain, M.; Opal, S. M. Clinical review: the role of biomarkers in the diagnosis and management of community-acquired pneumonia. *Crit Care* **2010**, *14* (1), 203–214.
- (6) Wunderink, R. G. Surrogate markers and microbiologic end points. *Clin Infect Dis.* **2010**, *51* (1), S126–130.
- (7) Jacobsen, M.; Mattow, J.; Repsilber, D.; Kaufmann, S. H. Novel strategies to identify biomarkers in tuberculosis. *Biol Chem.* **2008**, *389* (5), 487–495.
- (8) Parida, S. K.; Kaufmann, S. H. The quest for biomarkers in tuberculosis. *Drug Discov Today* **2010**, *15* (3–4), 148–57.
- (9) Vincent, J. L.; de Souza Barros, D.; Cianferoni, S. Diagnosis, management and prevention of ventilator-associated pneumonia: an update. *Drugs* **2010**, *70* (15), 1927–1944.
- (10) Zhang, L.; Zhang, X.; Ma, Q.; Ma, F.; Zhou, H. Transcriptomics and proteomics in the study of H1N1 2009. *Genomics Proteomics Bioinf.* **2010**, *8* (3), 139–144.
- (11) Claus, R. A.; Otto, G. P.; Deigner, H. P.; Bauer, M. Approaching clinical reality: markers for monitoring systemic inflammation and sepsis. *Curr Mol Med.* **2010**, *10* (10), 227–235.
- (12) Weljie, A. M.; Dowlatabadi, R.; Miller, B. J.; Vogel, H. J.; Jirik, F. R. An inflammatory arthritis-associated metabolite biomarker pattern revealed by <sup>1</sup>H NMR spectroscopy. *J Proteome Res.* **2007**, *6* (9), 3456–3464.
- (13) Weljie, A. M.; Newton, J.; Mercier, P.; Carlson, E.; Slupsky, C. M. Targeted profiling: quantitative analysis of <sup>1</sup>H NMR metabolomics data. *Anal Chem.* **2006**, *78* (13), 4430–4442.
- (14) Trygg, J.; Holmes, E.; Lundstedt, T. Chemometrics in metabonomics. *J Proteome Res.* **2007**, *6* (2), 469–479.
- (15) Lindon, J. C.; Holmes, E.; Nicholson, J. K. Metabonomics Techniques and Applications to Pharmaceutical Research & Development. *Pharm Res.* **2006**, *23* (6), 1076–1088.
- (16) Bourne, R.; Himmelreich, U.; Sharma, A.; Mountford, C.; Sorrell, T. Identification of Enterococcus, Streptococcus, and Staphylococcus by multivariate analysis of proton magnetic resonance spectroscopic data from plate cultures. *J Clin Microbiol.* **2001**, *39* (8), 2916–2923.
- (17) Coen, M.; O'Sullivan, M.; Bubb, W. A.; Kuchel, P. W.; Sorrell, T. Proton nuclear magnetic resonance-based metabonomics for rapid diagnosis of meningitis and ventriculitis. *Clin Infect Dis.* **2005**, *41* (11), 1582–1590.
- (18) Slupsky, C. M.; Cheypesh, A.; Chao, D. V.; Fu, H.; Rankin, K. N.; Marrie, T. J.; Lacy, P. Streptococcus pneumoniae and Staphylococcus aureus pneumonia induce distinct metabolic responses. *J Proteome Res.* **2009**, *8* (6), 3029–3036.
- (19) Slupsky, C. M.; Rankin, K. N.; Fu, H.; Chang, D.; Rowe, B. H.; Charles, P. G.; McGeer, A.; Low, D.; Long, R.; Kunimoto, D.; Sawyer, M. B.; Fedorak, R. N.; Adamko, D. J.; Saude, E. J.; Shah, S. L.; Marrie, T. J. Pneumococcal pneumonia: potential for diagnosis through a urinary metabolic profile. *J Proteome Res.* **2009**, *8* (12), 5550–5558.
- (20) Ala-Korpela, M. Critical evaluation of <sup>1</sup>H NMR metabonomics of serum as a methodology for disease risk assessment and diagnostics. *Clin Chem Lab Med.* **2008**, *46* (1), 27–42.
- (21) Griffin, J. L. Understanding mouse models of disease through metabolomics. *Curr Opin Chem Biol.* **2006**, *10* (4), 309–315.
- (22) Brightbill, H. D.; Libraty, D. H.; Krutzik, S. R.; Yang, R. B.; Belisle, J. T.; Bleharski, J. R.; Maitland, M.; Norgard, M. V.; Plevy, S. E.; Smale, S. T.; Brennan, P. J.; Bloom, B. R.; Godowski, P. J.; Modlin, R. L. Host defense mechanisms triggered by microbial lipoproteins through toll-like receptors. *Science* **1999**, *285* (5428), 732–736.
- (23) Takeuchi, O.; Hoshino, K.; Kawai, T.; Sanjo, H.; Takada, H.; Ogawa, T.; Takeda, K.; Akira, S. Differential roles of TLR2 and TLR4 in recognition of Gram-negative and Gram-positive bacterial cell wall components. *Immunity* **1999**, *11* (4), 443–451.
- (24) Hoshino, K.; Takeuchi, O.; Kawai, T.; Sanjo, H.; Ogawa, T.; Takeda, Y.; Takeda, K.; Akira, S. Cutting edge: Toll-like receptor 4 (TLR4)-deficient mice are hyporesponsive to lipopolysaccharide: evidence for TLR4 as the LPS gene product. *J Immunol.* **1999**, *162* (7), 3749–3752.
- (25) Bleasle, K.; Chen, Y.; Hellewell, P. G.; Burke-Gaffney, A. Lipoteichoic acid inhibits lipopolysaccharide-induced adhesion molecule expression and IL-8 release in human lung microvascular endothelial cells. *J Immunol.* **1999**, *163* (11), 6139–6147.
- (26) Alves-Filho, J. C.; Freitas, A.; Souto, F. O.; Spiller, F.; Paula-Neto, H.; Silva, J. S.; Gazzinelli, R. T.; Teixeira, M. M.; Ferreira, S. H.; Cunha, F. Q. Regulation of chemokine receptor by Toll-like receptor 2 is critical to neutrophil migration and resistance to polymicrobial sepsis. *Proc Natl Acad Sci U.S.A.* **2009**, *106* (10), 4018–4023.
- (27) Svensson, M.; Lohmeier-Vogel, E.; Waak, E.; Svensson, U.; Rådström, P. Altered nucleotide sugar metabolism in *Streptococcus thermophilus* interferes with nitrogen metabolism. *Int J Food Microbiol.* **2007**, *113* (2), 195–200.
- (28) Yipp, B. G.; Andonegui, G.; Howlett, C. J.; Robins, S. M.; Hartung, T.; Ho, M.; Kubes, P. Profound differences in leukocyte-endothelial cell responses to lipopolysaccharide versus lipoteichoic acid. *J Immunol.* **2002**, *168* (9), 4650–4658.
- (29) Andonegui, G.; Bonder, C. S.; Green, F.; Mullaly, S. C.; Zbytnuik, L.; Raharjo, E.; Kubes, P. Endothelium-derived Toll-like receptor 4 is the key molecule in LPS-induced neutrophil sequestration into lungs. *J Clin Invest.* **2003**, *111* (7), 1011–1020.
- (30) Krawisz, J. E.; Sharon, P.; Stenson, W. F. Quantitative assay for acute intestinal inflammation based on myeloperoxidase activity. Assessment of inflammation in rat and hamster models. *Gastroenterology* **1984**, *87* (6), 1344–1350.
- (31) Workentine, M. L.; Harrison, J. J.; Weljie, A. M.; Tran, V. A.; Stenroos, P. U.; Tremaroli, V.; Vogel, H. J.; Ceri, H.; Turner, R. J. Phenotypic and metabolic profiling of colony morphology variants evolved from *Pseudomonas fluorescens* biofilms. *Environ Microbiol.* **2010**, *12* (6), 1565–1577.
- (32) Shearer, J.; Duggan, G.; Weljie, A.; Hittel, D. S.; Wasserman, D. H.; Vogel, H. J. Metabolomic profiling of dietary-induced insulin resistance in the high fat-fed C57BL/6J mouse. *Diabetes Obes Metab.* **2008**, *10* (10), 950–958.
- (33) Nicholson, J. K.; Foxall, P. J.; Spraul, M.; Farrant, R. D.; Lindon, J. C. 750 MHz <sup>1</sup>H and <sup>1</sup>H-<sup>13</sup>C NMR spectroscopy of human blood plasma. *Anal Chem.* **1995**, *67* (5), 793–811.
- (34) Dieterle, F.; Ross, A.; Schlotterbeck, G.; Senn, H. Probabilistic quotient normalization as robust method to account for dilution of complex biological mixtures. Application in <sup>1</sup>H NMR metabonomics. *Anal Chem.* **2006**, *78* (13), 4281–4290.
- (35) Umetrics AB: Multi- Megavariate Data Analysis. Umea, Sweden 2001.
- (36) Dzurik, R.; Spustova, V.; Krivosikova, Z.; Gazdikova, K. Hippurate participates in the correction of metabolic acidosis. *Kidney Int.* **2001**, *59*, S278–281.
- (37) Cohen, P. P.; McGilvery, R. W. The formation of p-aminohippuric acid by liver homogenates. *J Biol Chem.* **1947**, *169* (1), 119–136.
- (38) Chantrenne, H. (1951). The requirement for coenzyme A in the enzymatic synthesis of hippuric acid. *J Biol Chem.* **1951**, *189* (1), 227–233.
- (39) Arends, J.; Chiu, F.; Bier, D. M. Analysis of plasma hippurate in humans using gas chromatography-mass spectroscopy: concentration and incorporation of infused [<sup>15</sup>N] glycine. *Anal Biochem.* **1990**, *191* (2), 401–410.

- (40) Arends, J.; Schäfer, G.; Schauder, P.; Bircher, J.; Bier, D. M. Comparison of serine and hippurate as precursor equivalents during infusion of [<sup>15</sup>N]glycine for measurement of fractional synthetic rates of apolipoprotein B of very-low-density lipoprotein. *Metabolism* **1995**, *44* (10), 1253–1258.
- (41) Schuller-Levis, G. B.; Park, E. Taurine and its chloramine: Modulators of immunity. *Neurochem. Res.* **2004**, *29* (1), 117–126.
- (42) Redmond, H. P.; Stapleton, P. P.; Neary, P.; Bouchier-Hayes, D. Immunonutrition: The role of taurine. *Nutrition* **1998**, *14* (7–8), 599–604.
- (43) Schicho, R.; Nazyrova, A.; Shaykhutdinov, R.; Duggan, G.; Vogel, H. J.; Storr, M. Quantitative metabolomic profiling of serum and urine in DSS-induced ulcerative colitis of mice by <sup>1</sup>H NMR spectroscopy. *J. Proteome Res.* **2010**, *9* (12), 6265–6273.
- (44) Duggan, G. E.; Hittel, D. S.; Hughey, C. C.; Weljie, A.; Vogel, H. J.; Shearer, J. Differentiating short- and long-term effects of diet in the obese mouse using <sup>1</sup>H-nuclear magnetic resonance metabolomics. *Diabetes Obes. Metab.* **2011**, *13* (9), 859–862.
- (45) Duggan, G. E.; Joan Miller, B.; Jirik, F. R.; Vogel, H. J. Metabolic profiling of vitamin C deficiency in *Gulo*−/− mice using proton NMR spectroscopy. *J. Biomol. NMR* **2011**, *49* (3–4), 165–173.
- (46) Duggan, G. E.; Hittel, D. S.; Sensen, C. W.; Weljie, A. M.; Vogel, H. J.; Shearer, J. Metabolomic response to exercise training in lean and diet-induced obese mice. *J. Appl. Physiol.* **2011**, *110* (5), 1311–1308.
- (47) Behrends, V.; Ebbels, T. M.; Williams, H. D.; Bundy, J. G. Time-resolved metabolic footprinting for nonlinear modeling of bacterial substrate utilization. *Appl. Environ. Microbiol.* **2009**, *75* (8), 2453–2463.
- (48) Krakauer, T. Immune response to staphylococcal superantigens. *Immunol. Res.* **1999**, *20* (2), 163–173.
- (49) Saric, J.; Li, J. V.; Swann, J. R.; Utzinger, J.; Calvert, G. Integrated cytokine and metabolic analysis of pathological responses to parasite exposure in rhodents. *J. Proteome Res.* **2010**, *9* (5), 2255–2264.
- (50) Gupta, R. K.; Yadav, S. K.; Rangan, M.; Rathore, R. K.; Thomas, M. A.; Prasad, K. N.; Pandey, C. M.; Saraswat, V. A. Serum proinflammatory cytokines correlate with diffusion tensor imaging derived metrics and <sup>1</sup>H-MR spectroscopy in patients with acute liver failure. *Metab. Brain Dis.* **2010**, *25* (3), 355–361.
- (51) Slack, A.; Yeoman, A.; Wendon, J. Renal dysfunction in chronic liver disease. *Crit. Care* **2010**, *14* (2), 214–224.
- (52) Pettersen, J.; Landaas, S.; Eldjarn, L. The occurrence of 2-hydroxybutyric acid in urine from patients with lactic acidosis. *Clin. Chim. Acta* **1973**, *48* (2), 213–219.
- (53) Wishart, D. S.; Tzur, D.; Knox, C.; Eisner, R.; Guo, A. C.; Young, N.; Cheng, D.; Jewell, K.; Arndt, D.; Sawhney, S.; Fung, C.; Nikolai, L.; Lewis, M.; Coutouly, M. A.; Forsythe, I.; Tang, P.; Srivastava, S.; Jeroncic, K.; Stothard, P.; Amegbey, G.; Block, D.; Hau, D. D.; Wagner, J.; Miniaci, J.; Clements, M.; Gebremedhin, M.; Guo, N.; Zhang, Y.; Duggan, G. E.; Macinnis, G. D.; Weljie, A. M.; Dowlatabadi, R.; Bamforth, F.; Clive, D.; Greiner, R.; Li, L.; Marrie, T.; Sykes, B. D.; Vogel, H. J.; Querengesser, L. HMDB: the human metabolome database. *Nucleic Acids Res.* **2007**, *35*, D521–D526.
- (54) Kanehisa, M.; Goto, S. KEGG: kyoto encyclopedia of genes and genomes. *Nucleic Acids Res.* **2000**, *28* (1), 27–30.
- (55) Pita, A. M.; Wakabayashi, Y.; Fernandez-Bustos, M. A.; Virgili, N.; Riudor, E.; Soler, J.; Farriol, M. Plasma urea-cycle-related amino acids, ammonium levels, and urinary orotic acid excretion in short-bowel patients managed with an oral diet. *Clinical Nutrition* **2003**, *22* (1), 93–98.
- (56) Yeung, D.; Oliver, I. T. Gluconeogenesis from amino acids in neonatal rat liver. *Biochem. J.* **1967**, *103* (3), 744–748.
- (57) Marshall, S.; Monzon, R. Amino acid regulation of insulin action in isolated adipocytes. Selective ability of amino acids to enhance both insulin sensitivity and maximal insulin responsiveness of the protein synthesis system. *J. Biol. Chem.* **1989**, *264* (4), 2037–2042.
- (58) Sweatt, A. J.; Garcia-Espinosa, M. A.; Wallin, R.; Hutson, S. M. Branched-chain amino acids and neurotransmitter metabolism: expression of cytosolic branched-chain aminotransferase (BCATc) in the cerebellum and hippocampus. *J. Comp. Neurol.* **2004**, *477* (4), 360–370.
- (59) Gilman, S. C.; Bonner, M. J.; Pellmar, T. C. Effect of oxidative stress on excitatory amino acid release by cerebral cortical synaptosomes. *Free Radic. Biol. Med.* **1993**, *15* (6), 671–675.
- (60) Kakazu, E.; Kanno, N.; Ueno, Y.; Shimosegawa, T. Extracellular branched-chain amino acids, especially valine, regulate maturation and function of monocyte-derived dendritic cells. *J. Immunol.* **2007**, *179* (10), 7137–7146.
- (61) Bell, J. D.; Lee, J. A.; Lee, H. A.; Sadler, P. J.; Wilkie, D. R.; Woodham, R. H. Nuclear magnetic resonance studies of blood plasma and urine from subjects with chronic renal failure: identification of trimethylamine-N-oxide. *Biochim. Biophys. Acta* **1991**, *1096* (2), 101–107.